

Coherent epitaxy of trilayer nickelate $(\text{Nd}_{0.8}\text{Sr}_{0.2})_4\text{Ni}_3\text{O}_{10}$ films by high-pressure magnetron sputtering

Jiachang Bi,^{1,2,3,*} Yujuan Pei,^{4,*} Ruyi Zhang,^{1,2} Shaoqin Peng,¹ Xinming Wang,¹ Jie Sun,¹ Jiagui Feng,⁵ Jingkai Yang,^{6,†} and Yanwei Cao^{1,2,‡}

¹*Ningbo Institute of Materials Technology and Engineering, Chinese Academy of Sciences, Ningbo, China*

²*Center of Materials Science and Optoelectronics Engineering,
University of Chinese Academy of Sciences, Beijing, China*

³*School of Future Technology, University of Chinese Academy of Sciences, Beijing, China*

⁴*School of Physics, Harbin Institute of Technology, Harbin, China*

⁵*Suzhou Institute of Nano-Tech and Nano-Bionics, Chinese Academy of Sciences, Suzhou, China*

⁶*Key Laboratory of Applied Chemistry, Hebei Key Laboratory of heavy metal deep-remediation in water and resource reuse,
College of Environmental and Chemical Engineering, Yanshan University, Qinhuangdao, China*

(Dated: November 5, 2021)

Rare-earth (R) nickelates (such as perovskite RNiO_3 , trilayer $\text{R}_4\text{Ni}_3\text{O}_{10}$, and infinite layer RNiO_2) have attracted tremendous interest very recently. However, unlike widely studied RNiO_3 and RNiO_2 films, the synthesis of trilayer nickelate $\text{R}_4\text{Ni}_3\text{O}_{10}$ films is rarely reported. Here, single-crystalline $(\text{Nd}_{0.8}\text{Sr}_{0.2})_4\text{Ni}_3\text{O}_{10}$ epitaxial films were coherently grown on SrTiO_3 substrates by high-pressure magnetron sputtering. The crystal and electronic structures of $(\text{Nd}_{0.8}\text{Sr}_{0.2})_4\text{Ni}_3\text{O}_{10}$ films were characterized by high-resolution X-ray diffraction and X-ray photoemission spectroscopy, respectively. The electrical transport measurements reveal a metal-insulator transition near 82 K and negative magnetoresistance in $(\text{Nd}_{0.8}\text{Sr}_{0.2})_4\text{Ni}_3\text{O}_{10}$ films. Our work provides a novel route to synthesize high-quality trilayer nickelate $\text{R}_4\text{Ni}_3\text{O}_{10}$ films.

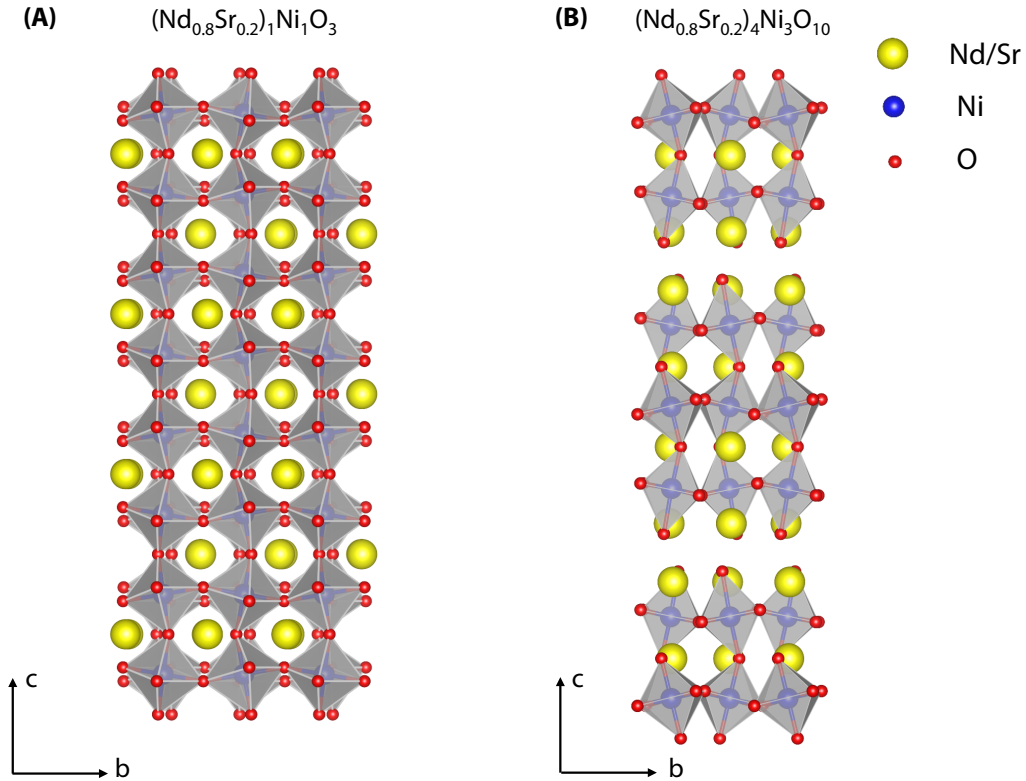


Figure 1. Schematic crystal structures of (A) NSNO₁₁₃ and (B) NSNO₄₃₁₀.

1. INTRODUCTION

Transition metal oxides with strong entanglements among spin, charge, orbital, and lattice degrees of freedom conceive a large number of emergent phenomena such as high-temperature superconductivity, colossal magnetoresistance, room-temperature multiferrocity, and metal-insulator transition[1–6]. One remarkable example of these transition metal oxides is the Rare-earth (R) nickelates in which metal-insulator transition, magnetic transition, and crystal structural transition were observed in perovskite nickelate RNiO₃[7–12], whereas the superconductivity (~ 15 K) presents in the infinite-layer nickelate RNiO₂ with doping [13–20]. Unlike comprehensively studied RNiO₃ and RNiO₂ films[21–27], the exploring of trilayer nickelate R₄Ni₃O₁₀ films is very rare[14, 28].

To address the above concern, we take (Nd_{0.8}Sr_{0.2})₄Ni₃O₁₀ (NSNO₄₃₁₀) films as a representative material to investigate the synthesis and the properties of R₄Ni₃O₁₀. The trilayer nickelate R₄Ni₃O₁₀ belongs to the $n = 3$ member of the Ruddlesden-Popper (RP) series of R _{$n+1$} Ni _{n} O_{3 $n+1$} , which shows a rich phase diagram of novel quantum states [28]. For example, large hole Fermi surface can be observed in La₄Ni₃O₁₀, which is analogous to the Fermi surface of optimally hole-doped cuprates[29]. Besides this property, metal to metal transition, charge order, intertwined charge, and spin density wave were also shown in R₄Ni₃O₁₀ [30–35]. Additionally, in the reduced phase of R₄Ni₃O₁₀ (such as R₄Ni₃O₈, R = La, Nd, Pr), charge/spin stripes, charge-stripe fluctuations, and orbital polarization were seen [36–39]. It is noted that the synthesis of high-quality bulk single crystals has been a big challenge[40, 41] and only successful in two groups [33, 36–38, 42].

Here, high-quality NSNO₄₃₁₀ epitaxial films were synthesized on SrTiO₃ (STO) substrates by high-pressure magnetron

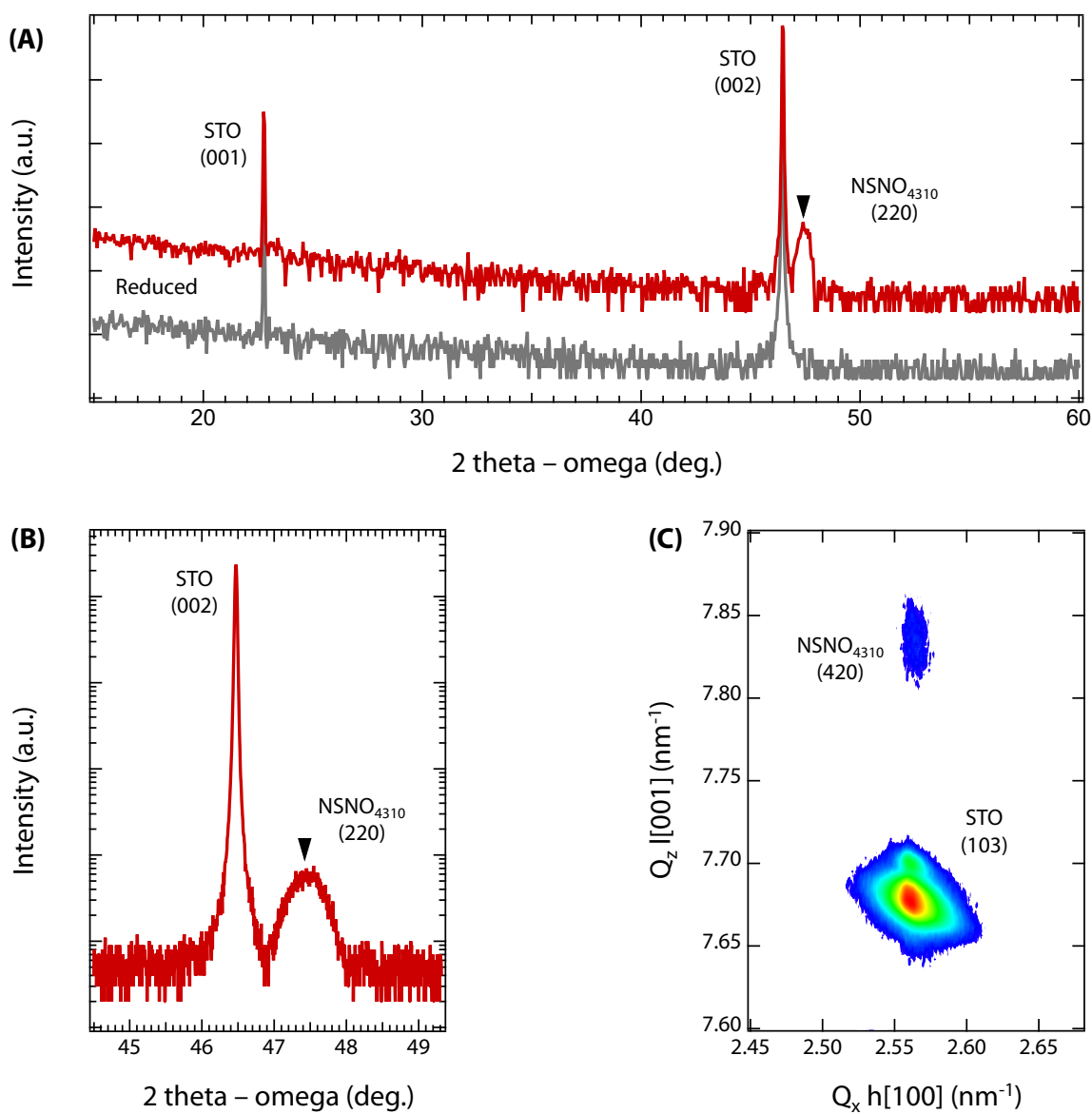


Figure 2. (A) Wide-range 2θ - ω scan of NSNO₄₃₁₀ (red) and NSNO₄₃₈ (grey) films along the STO (00L) diffraction. The black triangle indicates the (220) peak of NSNO₄₃₁₀ films. (B) Expanded view of Figure (A) near the STO (002) peak. (C) RSM pattern of NSNO₄₃₁₀ films (top) around asymmetric STO (103) diffraction (bottom).

sputtering. The crystal and electronic structures of NSNO₄₃₁₀ films were characterized by high-resolution X-ray diffraction (HRXRD) and X-ray photoemission spectroscopy (XPS). Electrical transport measurements reveal a metal-insulator transition (MIT) near 82 K and negative magnetoresistance. Our work provides a novel route to synthesize high-quality trilayer nickelate R₄Ni₃O₁₀ films.

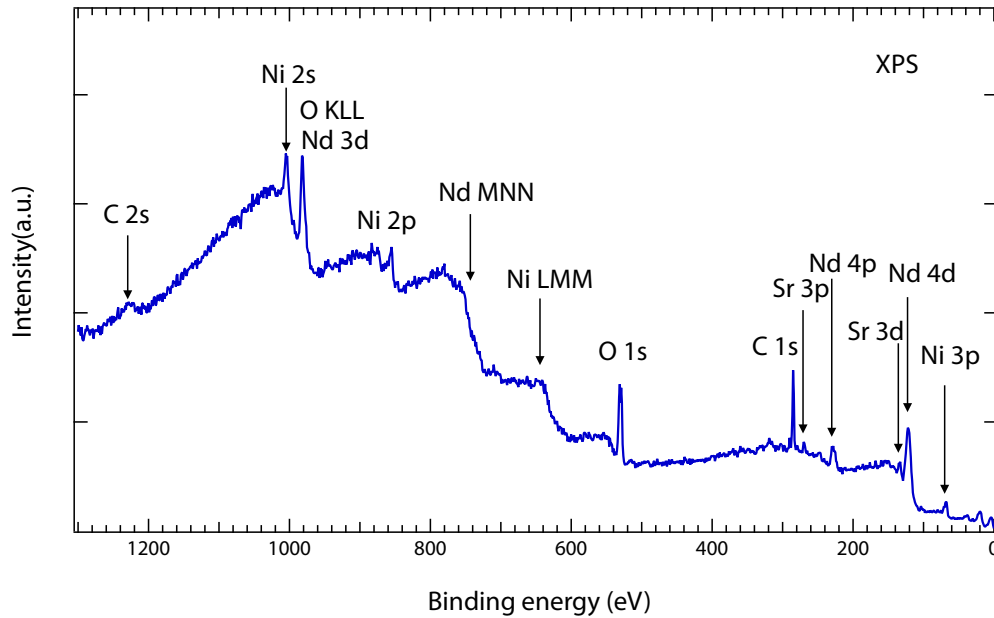


Figure 3. XPS spectra of NSNO₄₃₁₀ films on STO single-crystalline substrates at room temperature.

2. MATERIALS AND METHODS

2-inch Nd_{0.8}Sr_{0.2}NiO₃ polycrystalline targets were synthesized by a standard solid-state reaction method with initial reactants consist of Nd₂O₃ (Aladdin, 99.99%), SrCO₃ (Aladdin, 99.99%), and NiO (Aladdin, 99.99%). The mixture was calcined at 1350 °C for 8 h and reground for 6 h. Then the powders were pressed into a 2-inch target with 30 MPa and annealed at 1300 °C for 2 h. The high-quality NSNO₄₃₁₀ thin films (~20 nm) were synthesized by high-pressure radio frequency (RF) magnetron sputtering (home-made) with a 2-inch target and the O₂ (purity of 99.999%) reactive gas [43, 44]. Before growth, the base vacuum pressure was $\sim 3 \times 10^{-8}$ torr. During growth, O₂ pressure was kept at 0.02 Torr with a gas flow of 1.8 sccm, and the substrate temperature was held at 550 °C. The power of the RF generator was kept at 60 W. To ensure the uniformity of the films, the heating stage was rotating at a speed of 5 rams/min during growth. After growth, the films were cooled down to room temperature at 25 °C per minute in the 0.02 Torr O₂ atmosphere. A topochemical reduction process transforms NSNO₄₃₁₀ films into NSNO₄₃₈ films. The NSNO₄₃₈ films and reducing agent CaH₂ were sealed in an evacuated quartz tube and heated at 280 °C for 6 hours.

The crystal structure of NSNO₄₃₁₀ films was characterized by the High-resolution X-ray diffractometer (Bruker D8 Discovery) with the Cu K_α source ($\lambda = 1.5405 \text{ \AA}$). The 2θ - ω scans and asymmetrical reciprocal space mappings were performed to reveal the coherent growth and lattice parameters of films. The electronic structure of the films was probed by PHI 5000 Versa Probe x-ray photoelectron spectroscopy (XPS) at an acceptance angle of 45° for the analyzer (using monochromated Al K_α radiation, $h\nu = 1486.6 \text{ eV}$). The electrical properties were measured by Physical Property Measurement System (PPMS from Quantum Design) with four-point probe measurements.

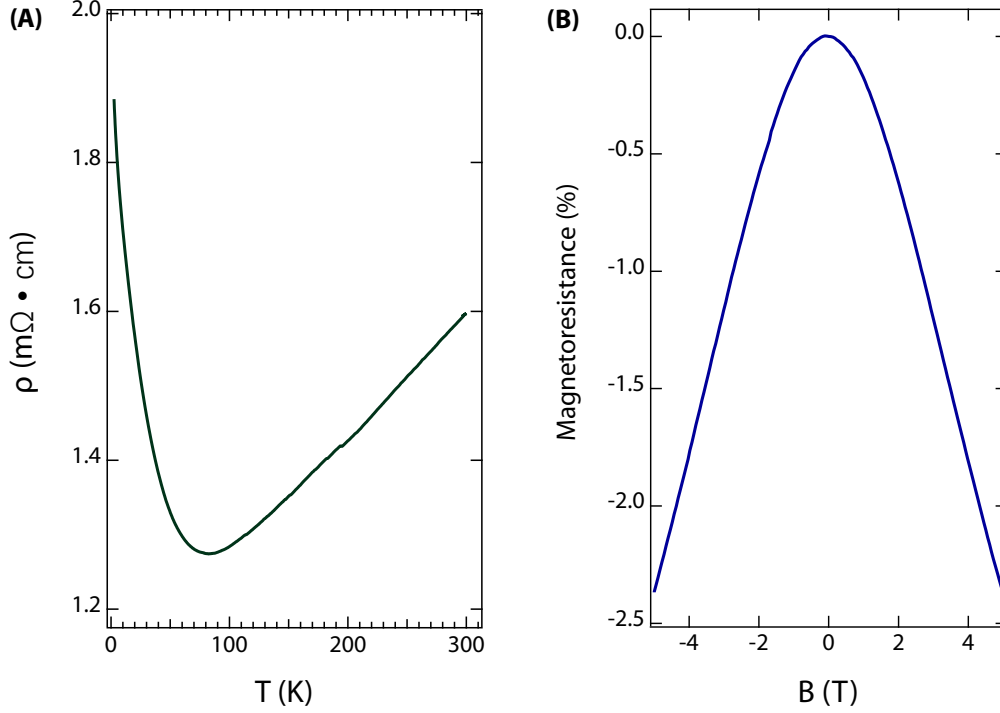


Figure 4. Transport properties NSNO₄₃₁₀ film. (a) Resistivity versus temperature ρ (T) curves from 2.5 K to 300 K. (b) Magnetoresistance $\Delta\rho/\rho_0$ at 2.5 K.

3. RESULTS AND DISCUSSIONS

Figure 1 shows the crystal structures of NSNO₁₁₃ and NSNO₄₃₁₀. NSNO₁₁₃ has a symmetry of orthorhombic structure with the lattice parameters $a = 5.39 \text{ \AA}$, $b = 5.38 \text{ \AA}$, $c = 7.61 \text{ \AA}$ (the pseudocubic lattice parameter is $\sim 3.81 \text{ \AA}$). It is noted that the replacement of Nd by Sr atoms via doping has little impact on the symmetry of crystal structure and the lattice parameters [45]. In contrast, the NSNO₄₃₁₀ has a monoclinic symmetry (space group $P2_1/a$) with the lattice parameters $a = 5.365 \text{ \AA}$, $b = 5.455 \text{ \AA}$, $c = 27.418 \text{ \AA}$, and $\beta = 90.31^\circ$ at room temperature [34, 46].

First, we performed HRXRD to characterize the crystal structure of NSNO₄₃₁₀ films. The wide-range 2θ - ω scans in Figure 2 (A) show that the (220) diffraction peak of NSNO₄₃₁₀ is along with the (00L) diffraction peaks of STO substrates without any secondary phases, whereas the (110) peak disappears due to the symmetry [46], indicating that NSNO₄₃₁₀ film is highly textured on STO substrates. The amplified view near (002) diffraction of STO substrates (see Figure 2 (B)) shows a film peak $\sim 47.46^\circ$, corresponding to a (110) layer spacing ($\sim 3.828 \text{ \AA}$) of NSNO₄₃₁₀ films, which agree well with the results in the literature [14, 46]. Reducing NSNO₄₃₁₀ films by CaH₂ can generate (Nd_{0.8}Sr_{0.2})₄Ni₃O₈ (NSNO₄₃₈) with diffraction angle at $\sim 46.47^\circ$, which is too close to the STO (002) peak near 46.47° to be seen [14, 47]. Hence, no significant feature is observed in Figure 2 (A) for NSNO₄₃₈ films.

Next, to characterize the in-plane lattice parameters of NSNO₄₃₁₀ films, we measured the reciprocal space mapping (RSM). Figure 2 (C) shows the RSM recorded around asymmetric STO (103) diffraction. The reciprocal lattice vectors Q_x and Q_z

correspond to the in-plane (100) and out-of-plane (001) directions of STO single crystalline substrates. The lower diffraction peak can be assigned to the STO, whereas the upper diffraction peak corresponds to the epitaxial NSNO₄₃₁₀. The epitaxial relationship can be expressed as, NSNO₄₃₁₀[1-10]//STO[100] and NSNO₄₃₁₀[001]//STO[010] for in-plane direction and NSNO₄₃₁₀(110)//STO(001) for out-of-plane direction. As revealed by RSM, NSNO₄₃₁₀ film shares the same Q_x value with that of STO substrates, indicating a coherent epitaxial growth for NSNO₄₃₁₀ film with an in-plane (1-10) layer spacing ~ 3.905 Å. From RSM, it is estimated that the (110) layer spacing is ~ 3.828 Å, agreeing very well with the value extracted from the (220) diffraction peak of NSNO₄₃₁₀ films. Thus, the RSM data further confirms the high-quality of epitaxial NSNO₄₃₁₀ films.

To further characterize the chemical composition of the NSNO₄₃₁₀ film, the XPS characterization was carried out. Figure 3 shows a wide-energy core-level XPS spectrum from 0 to 1300 eV. As seen, besides adsorbed carbon on the NSNO₄₃₁₀ film surface, no detectable impurity signal is observed.

Figure 4 (A) shows the temperature-dependent resistivity of NSNO₄₃₁₀ films from 2.5 K ($1.88 m\Omega \cdot cm$) to 300 K ($1.59 m\Omega \cdot cm$). There is a metal-insulator transition at ~ 82 K. It is noted that the resistivity remains small at the range of 2.5 - 300 K, indicating a metallic behavior. Magnetoresistance ($MR = \Delta\rho/\rho_0 \times 100\%$) at 2.5 K was also measured (see Figure 4 (B)). The negative magnetoresistance of NSNO₄₃₁₀ films has also been observed in the bulk [48], resulting from the weak localization at low temperature and being different from the electrical behavior of La₄Ni₃O₁₀[49] and Pr₄Ni₃O₁₀[33].

4. CONCLUSION

In this work, high-quality (Nd_{0.8}Sr_{0.2})₄Ni₃O₁₀ films have been synthesized on SrTiO₃ by high-pressure magnetron sputtering. The crystal and electronic structures of (Nd_{0.8}Sr_{0.2})₄Ni₃O₁₀ films are characterized by XRD and XPS. The electrical transport measurements reveal a metal-insulator transition and negative magnetoresistance. Our work provides a novel route to synthesize high-quality trilayer nickelate R₄Ni₃O₁₀ films.

ACKNOWLEDGMENTS

The authors deeply acknowledge the insightful discussions with Liang Wu. This work is supported by the National Natural Science Foundation of China (Grant Nos. 11874058 and U2032126), the Pioneer Hundred Talents Program of the Chinese Academy of Sciences, the Natural Science Foundation of Zhejiang Province, the Beijing National Laboratory for Condensed Matter Physics, and the Ningbo Science and Technology Bureau (Grant No. 2018B10060). This work is partially supported by the Youth Program of the National Natural Science Foundation of China (Grant No. 12004399), China Postdoctoral Science Foundation (Grant No. 2018M642500), and Postdoctoral Science Foundation of Zhejiang Province (Grant No. zj20180048).

* These authors contributed equally to this work

† yangjk@ysu.edu.cn

‡ ywcao@nimte.ac.cn

[1] Damascelli A, Hussain Z, Shen Z-X. Angle-resolved photoemission studies of the cuprate superconductors. *Rev. Mod. Phys.* (2003) 75:473. doi:10.1103/RevModPhys.75.473

- [2] Salamon MB, Jaime M. The physics of manganites: Structure and transport. *Rev. Mod. Phys.* (2001) 73:583. doi:10.1103/RevModPhys.73.583
- [3] Ramirez AP. Colossal magnetoresistance. *J. Phys.: Condens. Matter* (1997) 9:8171. doi:10.1088/0953-8984/9/39/005
- [4] Dawber M, Rabe KM, Scott JF. Physics of thin-film ferroelectric oxides. *Rev. Mod. Phys.* (2005) 77:1083. doi:10.1103/RevModPhys.77.1083
- [5] Martin LW, Rappe AM. Thin-film ferroelectric materials and their applications. *Nat. Rev. Mater.* (2017) 2:16087. doi:10.1038/natrevmats.2016.87
- [6] Imada M, Fujimori A, Tokura Y. Metal-insulator transitions. *Rev. Mod. Phys.* (1998) 70:1039. doi:10.1103/RevModPhys.70.1039
- [7] Liu J, Kareev M, Meyers D, Gray B, Ryan P, Freeland JW, et al. Metal-insulator transition and orbital reconstruction in Mott-type quantum wells made of NdNiO₃. *Phys Rev Lett.* (2012) 109:107402. doi:10.1103/PhysRevLett.109.107402
- [8] Chakhalian J, Rondinelli JM, Liu J, Gray BA, Kareev M, Moon EJ, et al. Asymmetric Orbital-Lattice Interactions in Ultrathin Correlated Oxide Films. *Phys Rev Lett.* (2011) 107:116805. doi:10.1103/PhysRevLett.107.116805
- [9] Middey S, Meyers D, Kareev M, Cao Y, Liu X, Shafer P, et al. Disentangled Cooperative Orderings in Artificial Rare-Earth Nickelates. *Phys Rev Lett.* (2018) 120:156801. doi:10.1103/PhysRevLett.120.156801
- [10] Liu J, Kargarian M, Kareev M, Gray B, Ryan PJ, Cruz A, et al. Heterointerface engineered electronic and magnetic phases of NdNiO₃ thin films. *Nat. Commun.* (2013) 4:2714. doi:10.1038/ncomms3714
- [11] Li J, Pellicciari J, Mazzoli C, Catalano S, Simmons F, Sadowski JT, et al. Scale-invariant magnetic textures in the strongly correlated oxide NdNiO₃. *Nat. Commun.* (2019) 10:4568. doi:10.1038/s41467-019-12502-0
- [12] Georgescu AB, Peil OE, Disa AS, Georges A, Millis AJ. Disentangling lattice and electronic contributions to the metal-insulator transition from bulk vs. layer confined RNiO₃. *Proc. Natl. Acad. Sci. U.S.A.* (2019) 116: 14434-39. doi:10.1073/pnas.1818728116
- [13] Li D, Lee K, Wang BY, Osada M, Crossley S, Lee HR, et al. Superconductivity in an infinite-layer nickelate. *Nature* (2019) 572:624-7. doi:10.1038/s41586-019-1496-5
- [14] Lee K, Goodge BH, Li D, Osada M, Wang BY, Cui Y, et al. Aspects of the synthesis of thin film superconducting infinite-layer nickelates. *APL Mater.* (2020) 8:041107. doi:10.1063/5.0005103
- [15] Hepting M, Li D, Jia CJ, Lu H, Paris E, Tseng Y, et al. Electronic structure of the parent compound of superconducting infinite-layer nickelates. *Nat. Mater.* (2020) 19:381-5. doi:10.1038/s41563-019-0585-z
- [16] Osada M, Wang BY, Goodge BH, Lee K, Yoon H, Sakuma K, et al. A Superconducting Praseodymium Nickelate with Infinite Layer Structure. *Nano Lett.* (2020) 20:5735-40. doi:10.1021/acs.nanolett.0c01392
- [17] Gao J, Peng S, Wang Z, Fang C, Weng H. Electronic structures and topological properties in nickelates Ln_{n+1}Ni_nO_{2n+2}. *Natl. Sci. Rev* (2020) nwa218. doi:10.1093/nsr/nwa218
- [18] Been E, Lee WS, Hwang HY, Cui Y, Zaanen J, Devereaux T, et al. Electronic Structure Trends Across the Rare-Earth Series in Superconducting Infinite-Layer Nickelates. *Phys. Rev. X* (2021) 11:011050. doi:10.1103/PhysRevX.11.011050
- [19] Li D. The discovery and research progress of the nickelate superconductors. *SCIENTIA SINICA Physica, Mechanica & Astronomica* (2021) 51:047405. doi:10.1360/SSPMA-2020-0396
- [20] Botana AS, Bernardini F, Cano A. Nickelate superconductors: an ongoing dialog between theory and experiments. *J. Exp. Theor. Phys.* (2021) 132:618-27. doi:10.1134/S1063776121040026
- [21] Li J, Green RJ, Zhang Z, Sutarto R, Sadowski JT, Zhu Z, et al. Sudden Collapse of Magnetic Order in Oxygen-Deficient Nickelate Films. *Phys. Rev. Lett.* (2021) 126:187602. doi:10.1103/PhysRevLett.126.187602
- [22] Wan X, Ivanov V, Resta G, Leonov I, Savrasov SY. Exchange interactions and sensitivity of the Ni two-hole spin state to Hund's coupling in doped NdNiO₂. *Phys. Rev. B* (2021) 103:075123. doi:10.1103/PhysRevB.103.075123
- [23] Wang Le, Yang Z, Yin X, Taylor SD, He X, Tang CS, et al. Spontaneous phase segregation of Sr₂NiO₃ and SrNi₂O₃ during SrNiO₃ heteroepitaxy. *Sci. Adv.* (2021) 7:2866. doi:10.1126/sciadv.abe2866

- [24] Wang Le, Yang Z, Bowden ME, Freeland JW, Sushko PV, Spurgeon SR, et al. Hole-Trapping-Induced Stabilization of Ni⁴⁺ in SrNiO₃/LaFeO₃ Superlattices. *Adv. Mater.* (2020) 32:2005003. doi:10.1002/adma.202005003
- [25] Wang X, Ge C, Li G, Guo E-J, He M, Wang C, et al. A synaptic transistor with NdNiO₃. *Chin. Phys. B* (2020) 29:098101. doi:10.1088/1674-1056/aba60c
- [26] Liao Z, Skoropata E, Freeland JW, Guo E-J, Desautels R, Gao X, et al. Large orbital polarization in nickelate-cuprate heterostructures by dimensional control of oxygen coordination. *Nat. Commun.* (2019) 10:589. doi:10.1038/s41467-019-08472-y
- [27] Cao Y, Liu X, Kareev M, Choudhury D, Middey S, Meyers D, et al. Engineered Mott ground state in a LaTiO_{3-δ}/LaNiO₃ heterostructure. *Nat. Commun.* (2016) 7:10418. doi:10.1038/ncomms10418
- [28] Zhang J, Tao X. Review on quasi-2D square planar nickelates. *CrystEngComm* (2021) 23:3249-64. doi:10.1039/D0CE01880E
- [29] Li H, Zhou X, Nummy T, Zhang J, Pardo V, Pickett WE, et al. Fermiology and electron dynamics of trilayer nickelate La₄Ni₃O₁₀. *Nat. Commun.* (2017) 8:704. doi:10.1038/s41467-017-00777-0
- [30] Zhang Z, Greenblatt M. Synthesis, Structure, and Properties of Ln₄Ni₃O_{10-δ} (Ln = La, Pr, and Nd). *J Solid State Chem* (1995) 117:236-46. doi:10.1006/jssc.1995.1269
- [31] Carvalho MD, Cruz MM, Wattiaux A, Bassat JM, Costa FMA, Godinho M. Influence of oxygen stoichiometry on the electronic properties of La₄Ni₃O_{10±δ}. *J. Appl. Phys.* (2000) 88:544. doi:10.1063/1.373693
- [32] Zhang J, Phelan D, Botana AS, Chen Y-S, Zheng H, Krogstad M, et al. Intertwined density waves in a metallic nickelate. *Nat. Commun.* (2020) 11:6003. doi:10.1038/s41467-020-19836-0
- [33] Huangfu S, Jakub GD, Zhang X, Blacque O, Puphal P, Pomjakushina E, et al. Anisotropic character of the metal-to-metal transition in Pr₄Ni₃O₁₀. *Phys. Rev. B* (2020) 101:104104. doi:10.1103/PhysRevB.101.104104
- [34] Li B-Z, Wang C, Yang PT, Sun JP, Liu Y-B, Wu J, et al. Metal-to-metal transition and heavy-electron state in Nd₄Ni₃O_{10-δ}. *Phys. Rev. B* (2020) 101:195142. doi:10.1103/PhysRevB.101.195142
- [35] Rout D, Mudi SR, Hoffmann M, Spachmann S, Klingeler R, Singh S. Structural and physical properties of trilayer nickelates R₄Ni₃O₁₀ (R = La, Pr and Nd). *Phys. Rev. B* (2020) 102:195144. doi:10.1103/PhysRevB.102.195144
- [36] Zhang J, Botana AS, Freeland JW, Phelan D, Zheng H, Pardo V. Large orbital polarization in a metallic square-planar nickelate. *Nat. Phys.* (2017) 13:864-9. doi:10.1038/nphys4149
- [37] Zhang J, Chen Y-S, Phelan D, Zheng H, Norman MR, Mitchell JF. Stacked charge stripes in the quasi-2D trilayer nickelate La₄Ni₃O₈. *Proc. Natl. Acad. Sci. U.S.A.* (2016) 113:8945-50. doi:10.1073/pnas.1606637113
- [38] Zhang J, Pajeroski DM, Botana AS, Zheng H, Harriger L, Rodriguez-Rivera J, et al. Spin Stripe Order in a Square Planar Trilayer Nickelate. *Phys. Rev. Lett.* (2019) 122:247201. doi:10.1103/PhysRevLett.122.247201
- [39] Hao J, Fan X, Li Q, Zhou X, He C, Dai Y, et al. Charge-stripe fluctuations in Nd₄Ni₃O₁₀ as evidenced by optical spectroscopy. *Phys. Rev. B* (2021) 103:205120. doi:10.1103/PhysRevB.103.205120
- [40] Das D, Pal M, Bartolomeo ED, Traversa E, Chakravorty D. Synthesis of nanocrystalline nickel oxide by controlled oxidation of nickel nanoparticles and their humidity sensing properties. *J. Appl. Phys.* (2000) 88:6856. doi:10.1063/1.1312835
- [41] Zinkevich M, Aldinger F. Thermodynamic analysis of the ternary La-Ni-O system. *J. Alloys Compd.* (2004) 375:147-61. doi:10.1016/j.jallcom.2003.11.138
- [42] Zhang J, Zheng H, Chen Y-S, Ren Y, Yonemura M, Huq A. High oxygen pressure floating zone growth and crystal structure of the metallic nickelates R₄Ni₃O₁₀ (R = La, Pr). *Phys. Rev. Mater.* (2020) 4:083402. doi:10.1103/PhysRevMaterials.4.083402
- [43] Zhang R, Ma Q-Y, Liu H, Sun T-Y, Bi J, Song Y, et al. Crystal Orientation-Dependent Oxidation of Epitaxial TiN Films with Tunable Plasmonics. *ACS Photonics* (2021) 8:847-56. doi:10.1021/acsp Photonics.0c01827.
- [44] Zhang R, Li X, Bi J, Zhang S, Peng S, Song Y, et al. One-step epitaxy of high-mobility La-doped BaSnO₃ films by high-pressure magnetron sputtering. *APL Mater.* (2021) 9:061103. doi:10.1063/5.0046639
- [45] García-Muñoz JL, Suaaidi M, Martínez-Lope MJ, Alonso JA. Influence of carrier injection on the metal-insulator transition in electron- and hole-doped R_{1-x}A_xNiO₃ perovskites. *Phys. Rev. B* (1995) 52:13563. doi:10.1103/PhysRevB.52.13563

- [46] Olafsen A, Fjellvåg H, Hauback BC. Crystal Structure and Properties of $Nd_4Ni_3O_{10+\delta}$ and $Nd_4Ni_3O_{10-\delta}$. *J. Solid State Chem* (2000) 151:46-55. doi:10.1006/jssc.2000.8620
- [47] Lacorre Ph. Passage from T-type to T'-type arrangement by reducing $R_4Ni_3O_{10}$ to $R_4Ni_3O_8$ ($R = La, Pr, Nd$). *J Solid State Chem* (1992) 97:495-500. doi:10.1016/0022-4596(92)90061-Y
- [48] Li Q, He CP, Zhu XY, Si J, Fan XW, Wen H-H. Contrasting physical properties of the trilayer nickelates $Nd_4Ni_3O_{10}$ and $Nd_4Ni_3O_8$. *SCI CHINA PHYS MECH* (2021) 64:227411. doi:10.1007/s11433-020-1613-3
- [49] Kumar S, Fjellvåg Ø, Sjøstad AO, Fjellvåg H. Physical properties of Ruddlesden-Popper (n=3) nickelate: $La_4Ni_3O_{10}$. *J. Magn. Magn. Mater.* (2020) 496:165915. doi:10.1016/j.jmmm.2019.165915